Modelling and Control of a Large Quadrotor Robot

P.Pounds*[,a], R.Mahony[b], P.Corke[c]

[a] *Yale University, 15 Prospect St, New Haven, CT 06511 USA*
[b] *Australian National University, Bld 32 North Road, Acton, ACT 0200 Australia*
[c] *Queensland University of Technology, Gardens Point, QLD 4001 Australia*

Abstract

Typical quadrotor aerial robots used in research weigh less than 3 kg and carry payloads measured in hundreds of grams. Several obstacles in design and control must be overcome to cater for expected industry demands that push the boundaries of existing quadrotor performance. The X-4 Flyer, a 4 kg quadrotor with a 1 kg payload, is intended to be prototypical of useful commercial quadrotors. The custom-built craft uses tuned plant dynamics with an onboard embedded attitude controller to stabilise flight. Independent linear SISO controllers were designed to regulate flyer attitude. The performance of the system is demonstrated in indoor and outdoor flight.

Key words: robotics, control, unmanned vehicles, aerospace, dynamics

1. Introduction

A major limitation of helicopters is the need for extensive, and costly, maintenance for reliable operation. Unmanned Air Vehicle (UAV) rotorcraft are no exception. Simplifying the mechanical structure of such craft clearly produces logistical benefits. Quadrotors are an alternative form of rotorcraft which do not have the complicated swashplates and linkages found in conventional designs, and instead use varying rotor speeds to manoeuver. Due to the great reduction of mechanical complexity and wear, it is expected that well-designed quadrotors will prove inherently more robust and reliable. However, for quadrotors to be competitive with helicopters for practical applications, it is desirable to maximise their dynamic performance and aerodynamic capabilites.

*Corresponding author

Quadrotors have been the subject of significant study since gaining the attention of robotics researchers in the early 2000s, and numerous papers have been written concerning their dynamics and describing methods to regulate their flight. Most early research quadrotors were based on small flying hobby craft such as the HMX-4 and Draganflyer [Draganfly Innovations Inc, 2009]. They are powered by NiCd or Li-Poly cells and use rate feedback from MEMS gyros for damping but have no roll or pitch angle stability. Research quadrotors add automatic stability and use a variety of hardware and control schemes. Example quadrotors include Eidgenössische Technische Hochschule Zürich's 'OS4' [Bouabdallah *et al.*, 2004b], a belt-driven flyer with low-aspect ratio blades; CEA's 'X4-flyer'[1], a small quadrotor with four blades per motor [Guenard *et al.*, 2005] and Cornell's Autonomous Flying Vehicle, a large craft using hobby aeroplane propellers.

Although attractive for use in industry due to their inherent robustness and compact layout, there have been few inroads into the development of more capable quadrotor UAVs scaled for industrial use.

Previous attempts to construct larger, heavy quadrotor UAVs (eg. >3 kg or >1 m), such as the Hoverbot [Borenstein, 1992] and Cornell Autonomous Flying Vehicle 'AFV', were limited by external attachments and tethers needed for operation [Nice, 2004]. The 6 kg Hoverbot was built from four hobby helicopters joined at the tail. It could lift itself into the air, but never flew off its sensored test gimbal. The 6.2 kg AFV was custom-built with hobby propellers, motors, electronic speed controllers and lithium batteries. It used shaft encoders for closed-loop rotor speed control, and Kalman filters to perform inertial sensor bias estimation. It flew with tethered power, but flight damage prevented further testing.

In the commercial sphere, several groups announced plans to market 4-6 kg devices, but these did not manifest in products, whereas numerous examples of sub-2 kg craft are now readily available. The rarity of quadrotor UAVs larger than 3 kg can be attributed to the numerous design challenges encountered as the weight of the vehicle increases, and to the attendant engineering rigour that must be exercised to safeguard proportionally more fragile hardware.

The authors identify one of the next challenges for practical quadrotors as

[1]Although similarly named, the ANU X-4 Flyer and CEA X4-flyer are quite different craft.

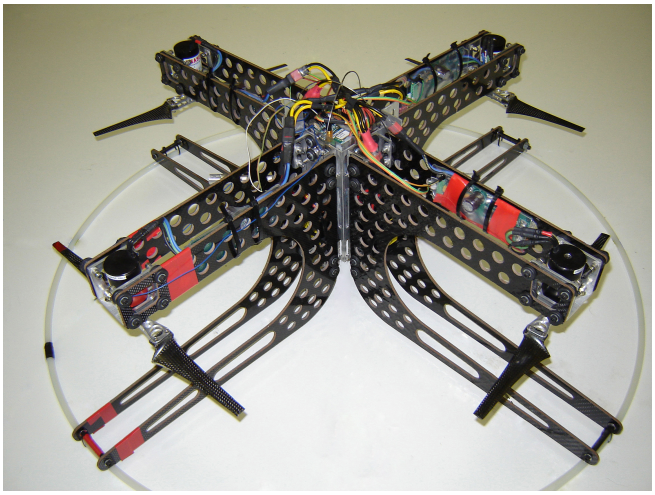

Figure 1: The X-4 Flyer.

being the maximisation of quadrotor aerodynamic and control performance to meet increasing demands of operators. While many tasks can be performed with small payloads and short flight-times, larger loads and longer flight-times represent greater utility for a commercial vehicle.

This challenge can be met by increasing the size and power of the vehicle. The thrust produced by a rotor is proportional to the fourth power of its radius and the square of its angular velocity. The input power required in hover is inversely proportional to radius, which motivates use of larger vehicles and higher power rotors for increased performance. The major limitations on helicopter size are structural, where rotors become so large that they droop towards the ground. The weight and dynamics of rotors have ramifications for the control performance that can be realised.

1.1. The X-4 Flyer

The Australian National University X-4 Flyer Mark III is a 4 kg quadrotor with a 1 kg payload[2]. It was designed to develop high thrust in a small footprint, with only 20 per cent larger area than the RCtoys Draganflyer IV (see Fig. 1). This was seen as a step towards highly capable industrial quadrotor UAVs. It uses custom high-performance rotors capable of lifting the

[2]It should be noted that there is no standard definition of payload. Carried weight can be added up to the maximum rotor thrust, at the expense of control margin.

flyer with an additional 30 per cent control margin (total thrust greater than 5.2 kg) [Pounds *et al.*, 2009]. The motors and batteries used are off-the-shelf components. The motors directly drive the rotors, eliminating the need for a gearbox. The robot has only eight moving parts – four pivoting rotor mounts and four motor hubs. As a result, the flyer is mechanically reliable with little scope for catastrophic failure in flight.

In this paper the critical control aspects of heavy quadrotors are reported: rotor speed control and attitude dynamic control. The dynamics of quadrotor helicopters with blade flapping are examined in detail. Based on the 6DOF aerodynamic model, decoupled dynamics in longitudinal (pitch/roll) and azimuthal modes are derived. We use this model to optimise the mechanical design of the X-4 Flyer for control of these dynamics and implement linear SISO control in the decoupled dynamics. The controller is tested on a gimbal rig and the performance realised in indoor and outdoor flight tests is reported. Findings are summarised with a brief conclusion.

2. Drive System

Efficient, compact, high-lift rotors are essential for quadrotor UAV application flight time and payload needs. Previous efforts to design drive systems have often consisted of an empirical approach, combining off-the-shelf parts [Bouabdallah *et al.*, 2004a] [Nice, 2004], but for best performance rotors and motors must be tuned to the specific needs of the aircraft. A method to design a complete drive system suitable for large quadrotors has been previously described [Pounds *et al.*, 2009]. In this section the essential facets of system design that apply to quadrotor control are reviewed.

2.1. Rotor Response Time

The swashplates of conventional helicopters allow instantaneous thrust changes, whereas most quadrotors use fixed-pitch rotors and must therefore accelerate and decelerate their rotors to manoeuver. As rotor size increases, mass and rotational inertia also increase. The rotor drive system must be capable of developing enough torque to affect prompt response. It is desirable to make the rotor and mast as light as possible to maximise actuator bandwidth.

In the case of the X-4 Flyer, it was found that the natural rise-time of the rotor mount, blade and motor assembly is 0.2 seconds, which made the

vehicle uncontrollable. Feedback control was required to reduce the response time to 0.05 seconds [Pounds *et al.*, 2009].

Especially large quadrotors may use collective variable blade pitch on each rotor and avoid the motor dynamics problem entirely. This was the approach taken by the Hoverbot [Borenstein, 1992]. The authors are not aware of any UAVs of this sort that have been flown, but it is expected that this is a viable alternative. However, collective blade control comes at the cost of increased mechanical complexity which abrogates the robustness advantage of simpler quadrotors.

2.2. Electronic Speed Control Hardware

Motor dynamic performance and robustness are crucial to quadrotor performance and reliability. Small quadrotors, such as the Draganflyer V, typically employ single power FETs modulating drive voltage to each permanent magnet DC motor. Larger craft employ brushless motors with electronic speed controllers (ESC). Properly engineered ESCs are required to extract maximum performance. Common practice has been to use off-the-shelf hobby aircraft ESCs because they are readily available and light weight. However, these have several drawbacks.

Most importantly for quadrotors, hobby controllers often have a built-in slew-limit designed to reduce the in-rush current draw upon step speed changes. Current spikes as high as 100 A have been measured in the X-4's drive [Pounds *et al.*, 2009]. Without slew limitation, the in-rush current can cause the power bus voltage to sag from internal resistance of the batteries, leading to avionics resetting, and severe spikes can even cause damage the ESC switching circuits. To avoid these problems, ESCs ramp speed changes slowly, increasing response time and limiting the bandwidth of the actuator. In the case of the X-4 Flyer, slew-limited hobby speed controllers could not respond fast enough to stabilise the craft.

Generally, hobby ESC microcontroller code and internals are inaccessible; no direct ESC rotor speed measurement is available externally, which may require additional sensors be added. It was found that high-gain, closed-loop speed control around the 50 Hz update rate of hobby RC equipment was not feasible for the X-4 Flyer. Programmable hobby ESCs now available can be hooked up to PCs for fine-tuning — these may be adaptable for large quadrotor speed control. However, a commercial high-performance quadrotor will almost certainly use custom drive electronics, as is the case with

the Ascending Technologies Hummingbird [Ascending Technologies GmbH, 2009].

2.3. Dynamic Compensation

Quadrotors must have fast thrust dynamics — the motors must be able to accelerate the rotors quickly to allow authorative attitude stabilisation. Most current quadrotors have light rotors that allow for fast speed changes without additional control. Large quadrotors have heavier, high inertia rotors and thus need local control to artificially improve the motor bandwidth. Reflected rotor inertia through any gearing should also be matched to the inertia of the motor to allow for maximum acceleration, although this must be balanced against the added mass, complexity and friction of a drive train. In practice, the closed-loop performance is most heavily constrained by limits on the available instantaneous current draw on the batteries and this dominates the control design.

Brushless motor speed dynamics are a single-pole dynamic system, and proportional feedback control is suitable. The control gain that can be realised by the torque-limited plant is bound by the maximum slew-rate that disturbance noise and sinusoidal references may demand without inducing failure in the controller. A method for calculating an optimised control design for a slew-saturated drive has been previously described [Pounds *et al.*, 2009].

Given sufficient bandwidth, the motor controller need not maintain precise rotor speed — the attitude control system for a full UAV will contain integral terms that will compensate motor set-points to ensure flight stability of the vehicle.

3. Quadrotor Dynamics

Mathematical dynamic models of flight behaviour are essential for good control design and analysis. A common model used to represent quadrotor behaviour is that of Hamel *et al* [Hamel *et al.*, 2002]. The most basic quadrotor model used consists only of rigid body dynamics with abstract force and torque actuators and no aerodynamics. The quadrotor is commonly represented as a rigid body mass with inertia and autogyroscopics, acted upon by gravity and control torques.

Simple quadrotor dynamic models do not represent the complex helicopter behaviour exhibited by real quadrotors. In particular, they omit the

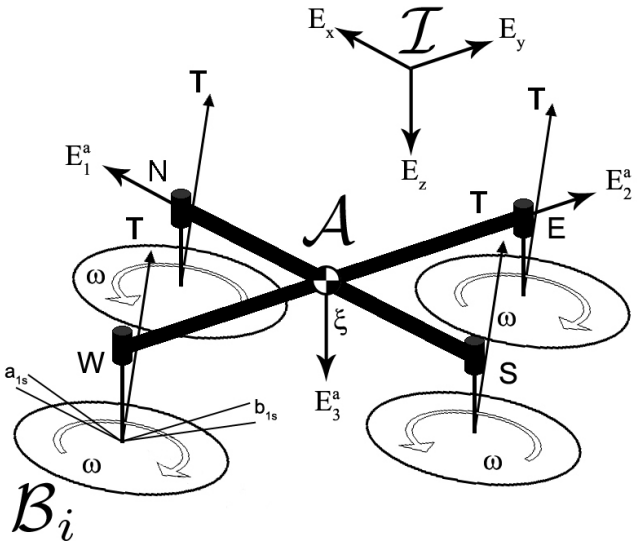

Figure 2: Flapping Quadrotor Free-body Diagram.

blade flapping effect, which is critical to understanding oscillatory helicopter modes, rotor flapping due to yaw and variable rotor inflow velocities as a result of craft pitch and roll.

Flapping dynamics are beginning to be recognised as important aspects of quadrotor dynamics; even very small quadrotors exhibit flapping [Huang *et al.*, 2009]. The nature of the instability of quadrotor dynamics, oscillatory or pure divergence, was shown to be dependent upon the height of the rotor above the centre of mass; setting the rotors to be on, or just above, the plane of the centre of gravity minimises the sensitivity function of the system [Pounds *et al.*, 2006]. In the case of large quadrotors, where actuator bandwidth is limited by slow rotor dynamics, this may be a crucial design point.

3.1. Rigid Body Dynamics

The inertial reference frame is denoted by $\mathcal{I}$= $\{E_x, E_y, E_z\}$, where E_z is in the direction of gravity, and $\xi = (x, y, z)$ is the origin of the body fixed frame $\mathcal{A}$ =$\{E^a_1, E^a_2, E^a_3\}$ where x is aligned with the front of the craft(see Fig. 2). The frame $\mathcal{A}$ is related to $\mathcal{I}$ by the rotation matrix $R : \mathcal{A} \rightarrow \mathcal{I}$. Vectors $\mathbf{v}$ and $\boldsymbol{\omega}$ are the linear and angular velocities of the frame in $\mathcal{A}$.

The equations are:

$$\dot{\xi} = \mathbf{R}\mathbf{v} \tag{1}$$

$$m\dot{\mathbf{v}} = -m\boldsymbol{\omega} \times \mathbf{v} + mg\mathbf{R}^{\mathrm{T}} e_3 + \sum_{N,S,E,W} \mathbf{t}_i \tag{2}$$

$$\dot{\mathbf{R}} = \mathbf{R} \cdot \mathrm{sk}\left(\boldsymbol{\omega}\right) \tag{3}$$

$$\mathbf{I}\dot{\boldsymbol{\omega}} = -\boldsymbol{\omega} \times \mathbf{I}\boldsymbol{\omega} + \sum_{N,S,E,W} \left[\mathbf{q}_i + \mathbf{m}_i\right] \tag{4}$$

$$\mathbf{t}_i = C_{\mathrm{T}} \rho A r^2 \omega_i^2 \begin{pmatrix} -\sin a_{1_s i} \\ \cos a_{1_s i} \sin b_{1_s i} \\ -\cos b_{1_s i} \cos a_{1_s i} \end{pmatrix} \tag{5}$$

$$\mathbf{q}_i = C_{\mathrm{Q}} \rho A r^3 \omega_i |\omega_i| e_3 \tag{6}$$

$$\mathbf{m}_i = \mathbf{t}_i \times \mathbf{d}_i \tag{7}$$

where m and $\mathbf{I}$ are the mass and rotational inertia of the flyer, g is acceleration due to gravity, ρ is the density of air, r is the rotor radius, and A is the rotor disc area. In equation 6, ω is multiplied by its magnitude to preserve the sign of rotation for counter-rotating rotors.

Here $\mathrm{sk}(x)$ is the skew-symmetric matrix such that $\mathrm{sk}(a)b = a \times b$ for vectors in $\Re^3$.

Rotors are indexed by their corresponding compass directions: North, South, East and West ($NSEW$), where N indicates the front rotor. Correspondingly, $\mathbf{d}_i$ is the rotor displacement from the flyer centre of mass:

$$\mathbf{d}_N = \begin{pmatrix} 0 & d & h \end{pmatrix} \tag{8}$$

$$\mathbf{d}_S = \begin{pmatrix} 0 & -d & h \end{pmatrix} \tag{9}$$

$$\mathbf{d}_E = \begin{pmatrix} d & 0 & h \end{pmatrix} \tag{10}$$

$$\mathbf{d}_W = \begin{pmatrix} -d & 0 & h \end{pmatrix} \tag{11}$$

where d is the arm length of the flyer and h is the height of the rotors above the CoG.

Vectors $\mathbf{t}_i$ and $\mathbf{q}_i$ are the rotor thrust and torque, and $\mathbf{m}_i$ is the moment due to the thrust vector of the ith rotor — for a teetering rotor, the moment produced by the rotor flapping is due solely to the thrust vector acting around a displacement from the vehicle's centre of gravity. The first harmonics of the longitudinal and lateral flapping angles of the ith rotor are denoted by a_{1s_i} and b_{1s_i}, respectively. The non-dimensionalised thrust and torque

coefficients, C_{T} and C_{Q}, are treated as constants here. The speed of the ith rotor is given by ω_i. The non-dimensionalised thrust coefficient and flapping equations are discussed in more detail in Sections 3.2 and 3.3.

3.2. Pitch and Roll Rotor Damping

A quadrotor necessarily has a horizontal displacement between its masts and CoG. When the craft rolls and pitches, the rotors experience a vertical velocity, leading to a change in the inflow angle. From Prouty [Prouty, 2002, p 101], C_{T} can be related to the vertical velocity, V_c, by:

$$C_{\mathrm{T}}/\sigma = \frac{a(\alpha)}{4}\left[\theta_{\mathrm{tip}} - \frac{v_i + V_c}{\omega r}\right] \tag{12}$$

where a is the airfoil polar lift slope, θ_{tip} is the geometric blade angle at the tip of the rotor, v_i is the induced velocity through the rotor, and σ is the solidity of the disc — the ratio of the surface area of the blades and the rotor disc area. The added lift due to increased flow velocity magnitude at the blade is small relative to the effect of changing inflow angle, and is ignored.

The polar lift slope is itself a function of the rotor blade angle of attack, α. It is highly nonlinear for some airfoils and so the relation can be better expressed as a variation around a set point, C_{T0}:

$$C_{\mathrm{T}i} = C_{\mathrm{T0}} + \Delta C_{\mathrm{T}i} \tag{13}$$

where ΔC_{T} is the change induced by the changing inflow conditions. From Equation 12, this is written as:

$$\Delta C_{\mathrm{T}i} = -\frac{a_0}{4}\frac{\sigma}{\omega_i r}(\mathbf{v} + \boldsymbol{\omega} \times \mathbf{d}_i)e_3 \tag{14}$$

where a_0 is the lift slope at the set point.

The inflow velocity of the X-4's rotors is very high with respect to pitch, roll and translation velocities. Consequently, the vehicle does not readily induce vortex ring states, even during aggressive manoeuvres.

3.3. Blade Flapping

When the rotors translate horizontally there is a difference in blade lift between the advancing and retreating blades, which causes the rotor tip path plane to tilt. The resulting angle of the rotor plane is obtained by simultaneously solving the constant and sinusoidal components of the blade

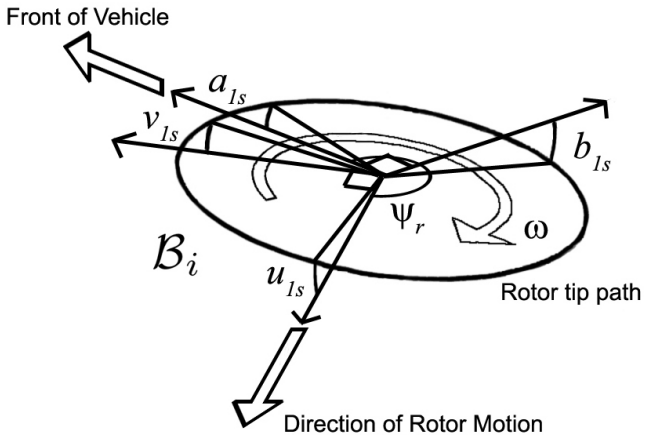

Figure 3: Blade Flapping Angle Rotation.

centrifugal-aerodynamic-static weight moment system. Flapping is important, as the tilting rotor can introduce significant stability effects for the vehicle [Pounds *et al.*, 2006].

The dynamics of rotor flapping are very fast, occurring within one revolution of the rotor [Leishman, 2006], compared with the rigid body dynamics of the helicopter. Consequently, the blade flapping equations can be written as instantaneous functions of the craft's planar velocity.

A quadrotor's flight is not limited to longitudinal motion – when the vehicle moves laterally or yaws the principal flapping axis need not be aligned to the front of the aircraft. The flapping of the ith rotor due to planar motion is found by calculating the magnitude and direction of rotor's translation and defining a local frame of reference, $\mathcal{B}_i$, aligned in that direction. The longitudinal and lateral flapping angles are calculated in the rotor frame ($u_{1_s i}$ and $v_{1_s i}$) and then re-expressed in the body-fixed frame ($a_{1_s i}$ and $b_{1_s i}$) using a rotation matrix (see Fig. 3). This allows the avoidance of computational complexity by using standard flapping equations in the local frame.

The per-rotor flapping is found by first computing the advance ratio and azimuthal direction of the rotor. This is derived as:

$$\mathbf{v}_{ri} = \mathbf{v} + \boldsymbol{\omega} \times \mathbf{d}_i \tag{15}$$

$$\mu_{ri} = \frac{\|\mathbf{v}_{r(1,2)i}\|}{\omega_i r} \tag{16}$$

$$\psi_{ri} = \arctan\left(\frac{\mathbf{v}_{r(2)i}}{\mathbf{v}_{r(1)i}}\right) \tag{17}$$

where $\mathbf{v}_{r(n)i}$ is the nth element of the ith rotor's velocity vector, μ_{ri} is the ith rotor's advance ratio and ψ_{ri} is the azimuthal direction of motion.

The X-4 uses a mechanical 'see-saw' teetering hinge and so has no flapping hinge offset. It also has no cyclic or collective blade control and so the classic equations [Prouty, 2002, p 469] can be greatly simplified: the longitudinal and lateral flapping angle solutions of the ith rotor in the local frame, $\mathcal{B}_i$, are:

$$u_{1_s i} = \frac{1}{1 - \frac{\mu_{ri}^2}{2}} \mu_{ri} \left(4\theta_t - 2\lambda_{\mathrm{h}i}^2\right) \tag{18}$$

$$v_{1_s i} = \frac{1}{1 + \frac{\mu_{ri}^2}{2}} \left(\frac{C_\mathrm{T}}{\sigma}\frac{8}{9}\frac{\mu_{ri}\gamma}{a} + \frac{C_\mathrm{T}}{2\mu_{ri}}\right) \tag{19}$$

respectively, where $\lambda_{\mathrm{h}i}$ is the non-dimensionalised near-hover inflow of the ith rotor [Leishman, 2006, pp 95], approximated by:

$$\lambda_{\mathrm{h}i} = \sqrt{C_\mathrm{T}/2} \tag{20}$$

and γ is the Lock Number [Leishman, 2006]:

$$\gamma = \frac{\rho a_0 c r^4}{I_b} \tag{21}$$

where I_b is the rotational inertia of the blade about the flapping hinge. Equation 18 substitutes blade tip angle for collective pitch angle and linear blade twist: $\theta_t = \frac{2}{3}\theta_0 + \frac{1}{2}\theta_l$, where θ_0 is the collective blade pitch and θ_l is the linear blade twist angle per meter.

These are transformed back into the body-fixed frame by ${}^{\mathcal{A}}\mathbf{J}_{\mathcal{B}_i}$, the frame mapping between $\mathcal{A}$ and $\mathcal{B}_i$, to derive the body-frame flapping angles due to

motion of the flyer:

$$ {}^{\mathcal{A}}\mathbf{J}_{\mathcal{B}_i} = \begin{pmatrix} \cos\psi_{ri} & -\sin\psi_{ri} \\ \sin\psi_{ri} & \cos\psi_{ri} \end{pmatrix} \tag{22} $$

$$ \begin{pmatrix} a_{1_s i} \\ b_{1_s i} \end{pmatrix} = {}^{\mathcal{A}}\mathbf{J}_{\mathcal{B}_i} \begin{pmatrix} u_{1_s i} \\ v_{1_s i} \end{pmatrix} \tag{23} $$

The components of the flapping angles produced by the craft's pitch and roll rates [Prouty, 2002, p 473] are added to those of the body-fixed frame:

$$ a_{1_s i} = \ldots + \frac{-\frac{16}{\gamma}\left(\frac{q}{\omega}\right) + \left(\frac{p}{\omega}\right)}{1 - \frac{\mu_i^2}{2}} \tag{24} $$

$$ b_{1_s i} = \ldots + \frac{-\frac{16}{\gamma}\left(\frac{p}{\omega}\right) + \left(\frac{p}{\omega}\right)}{1 + \frac{\mu_i^2}{2}} \tag{25} $$

4. Model Parameterisation and Stability

High-performance quadrotor attitude regulation poses additional challenges due to the need to consider more completely the dynamics expressed by rotorcraft and the difficulty in parameterising and testing controllers prior to flight. In this section the implications of large quadrotor dynamics and principal considerations for attitude controller design are discussed.

4.1. Parameterisation and Uncertainty

Robustness to plant uncertainty is essential for high-performance control. It is difficult to perform classic step response experiments to characterise the vehicle in flight prior to developing a basic stabilising controller — instability caused by erroneous control is liable to severely damage or destroy fragile craft.

Most of the plant model parameters are dictated by physical constants or the flight characteristics of the system; some, most importantly h, can be chosen freely. The error associated with each parameter defines the envelope of the plant model's dynamic response. The system behaviour within this envelope is analysed to determine the best value of h, the height of the rotors above the CoG.

A set of parameter estimates, taken directly from measurements or derived from experiments, are known along with the associated error. In the case of parameters computed from other known values, the associated errors were also computed:

- Aerodynamic parameters
  Rotor, blade and aerodynamic parameters are obtained through measurement, computation, simulation or from references. These are listed in Table 1.

- Masses and Displacements
  Component masses and distances measured with respect to the rotor plane, (masses ± 0.005 kg, distances ± 0.005 m) are given in Table 2. Note that this table is not a complete listing of all masses, but includes all major masses — screws and fasteners are omitted (see Fig. 4).

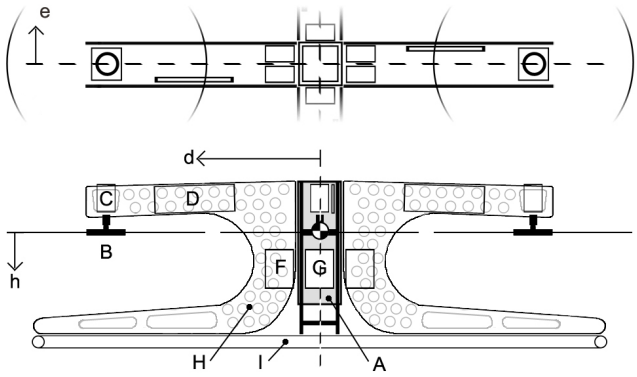

Figure 4: X-4 Component Offsets.

- Rotational Inertia
  Computed from the previous values by treating the parts as point masses, the diagonal entries of the inertial matrix are given in Table 3. The CoG is 0.0071 ± 0.005 m above the rotor plane.

4.2. Unforced Stability Analysis

The dominant dynamics of a helicopter, or a quadrotor, are associated with the longitudinal dynamics of the vehicle. Around hover, the motion of a helicopter is largely decoupled in each axis. The symmetry of quadrotors means that the important attitude dynamics can be described by a single equation.

The natural stability of these dynamics is analysed to provide insight into the best airframe geometry for controllability of the system. Prouty's stability analysis of the near-hover dynamics of helicopters is employed, with the addition of terms specific to quadrotors.

From the basic dynamic equations for a helicopter constrained to translate in x and rotate in pitch only without control inputs, the stability derivative matrix is [Prouty, 2002, p 564]:

$$\begin{vmatrix} -ms + \frac{\partial X}{\partial \dot{x}} & \frac{\partial X}{\partial \dot{\theta}} s - mg \\ \frac{\partial M}{\partial \dot{x}} & -I_{YY} s^2 + \frac{\partial M}{\partial \dot{\theta}} s \end{vmatrix} \begin{vmatrix} \dot{x} \\ \theta \end{vmatrix} = 0 \tag{26}$$

where x is the longitudinal position, θ is the pitch angle and s is the Laplace transform of the differential operator. The longitudinal force, X, and pitch moment, M, stability derivatives for a teetering hinge, fixed pitch rotor are:

$$\frac{\partial X}{\partial \dot{x}} = -\rho A(\omega_0 r)^2 \left(\frac{3}{2} \frac{C_\mathrm{T}}{\sigma} \left(1 - \frac{a}{12} \frac{\theta_t}{C_\mathrm{T}/\sigma} \right) \right) \frac{4\theta_t - 2\lambda_h}{\omega_0 r} \tag{27}$$

$$\frac{\partial X}{\partial \dot{\theta}} = -\rho A(\omega_0 r)^2 \left(\frac{3}{2} \frac{C_\mathrm{T}}{\sigma} \left(1 - \frac{a}{2} \frac{\theta_t}{C_\mathrm{T}/\sigma} \right) \right) \tag{28}$$

$$\frac{\partial M}{\partial \dot{x}} = -\frac{\partial X}{\partial \dot{x}} h \tag{29}$$

$$\frac{\partial M}{\partial \dot{\theta}} = \frac{\partial X}{\partial \dot{\theta}} h \tag{30}$$

For quadrotors, $\partial M/\partial \dot{x}$, and $\partial X/\partial \dot{x}$ are multiplied by 4 (for four rotors). A term is also added to $\partial M/\partial \dot{\theta}$ for the vertical motion of the rotors through their inflow in pitch and roll:

$$\frac{\partial M}{\partial \dot{\theta}} = \ldots - \rho A(\omega R)^2 2d \frac{\partial C_\mathrm{T}}{\partial \dot{\theta}} \tag{31}$$

where:

$$\frac{\partial C_\mathrm{T}}{\partial \dot{\theta}} = \frac{-a}{8} \sigma \frac{1}{\omega R} \tag{32}$$

The characteristic equation of the system matrix determinant, in canonical form of $As^3 + Bs^2 + Cs + D$, becomes:

$$s^3 - \left(\frac{1}{m} \frac{\partial X}{\partial \dot{x}} + \frac{1}{I_{YY}} \frac{\partial M}{\partial \dot{\theta}} \right) s^2 + \frac{g}{I_{YY}} \frac{\partial M}{\partial \dot{x}} = 0 \tag{33}$$

Solving for the roots of this polynomial gives the exponential components of the dynamic behaviour of the system.

Application of Routh's Discriminant, as outlined in Prouty, uses the coefficients of the characteristic polynomial, A, B, C and D, to determine the nature of the instability [Prouty, 2002, p 602]. From equation 33:

$$A = 1 \tag{34}$$

$$B = -\left(\frac{1}{m}\frac{\partial X}{\partial \dot{x}} + \frac{1}{I_{YY}}\frac{\partial M}{\partial \dot{\theta}}\right) \tag{35}$$

$$C = 0 \tag{36}$$

$$D = \frac{g}{I_{YY}}\frac{\partial M}{\partial \dot{x}} \tag{37}$$

The Routh's Discriminant, $R.D.$, is given by:

$$R.D. = BC - AD \tag{38}$$

If all coefficients are positive, there will be no pure divergence. If R.D. is positive, the craft will exhibit no unstable oscillation. If negative, the craft will exhibit unstable oscillation. If zero, the pitch dynamic will be neutral. As $C = 0$, there is no way to satisfy the first and second conditions simultaneously, and so the system cannot be made stable. Substituting the coefficients into equation 38 and simplifying, R.D. becomes:

$$R.D. = -C_{\mathrm{T}}\rho A\left(\omega r\right)^2 h \tag{39}$$

Of the composing terms, only h can change signs. For a conventional helicopter, where $h > 0$, the craft has an unstable pole pair. If the rotors are inverted (above the CoG), the craft will diverge without oscillation. If the rotors and CoG are coplanar, the craft is neutral.

4.3. Parameterised Model Envelope

Using the physical values for the X-4 Flyer, the coupled pitch and x translational dynamical equations can be computed. The error range of the parameters maps the roots of the plant into a space on the complex plane. Linearised differential equations for the flyer are taken from solving equations 1 – 25 for acceleration in pitch and x translation:

$$m\ddot{x} = -mga_{1_s} - mg\theta \tag{40}$$

$$I_{YY}\ddot{\theta} = 4dC_{\mathrm{T}}\rho Ar^2\omega_0\delta\omega + mga_{1_s}h - \frac{a}{2}\sigma\rho Ar\omega_0 d^2\dot{\theta} \tag{41}$$

These can be solved by substituting equations 23, 24 and 40 into 41, where equation 16 becomes $\dot{x}/(\omega_0 r)$, to produce a single transfer function $H = \theta/\delta\omega$ between pitch angle, θ, and the input differential change in rotor speeds, $\delta\omega$:

$$H = \frac{4dC_{\mathrm{T}}rc_2(s + gc_1)}{(s + gc_1)(I_{YY}s^2 - hmgc_3 s + \frac{a_0}{2}\sigma c_2 d^2 s) + hmg\,(gc_3 s - g))} \tag{42}$$

where:

$$c_1 = \frac{4\theta_t - 2\lambda}{\omega_0 r} \tag{43}$$

$$c_2 = \rho A r \omega_0 \tag{44}$$

$$c_3 = \frac{16}{\gamma\omega_0} \tag{45}$$

The flapping angle is approximated as a linear function of $\dot{x}$ and $\dot{\theta}$:

$$a_{1_s} = c_1\dot{x} + c_3\dot{\theta} \tag{46}$$

Using the system parameters and errors, the poles and zeros of the system are given in Table 4. The rotor height above the CoG is the predominant contributor to error, thus accurate knowledge of the rotor height is important to determining the dynamic model.

The unforced stability analysis demonstrated that h is also important in determining the behaviour of the dynamic system. The root locus for h shows that the structure of the open-loop poles changes significantly as h changes sign (see Fig. 5): the system exhibits an unstable oscillation when the CoG is below the rotor, pure divergence when it is above the rotor, and neutral stability when coincident with the rotor.

5. Design for Control

The use of automatic compensators no longer requires that a system be intuitive for a human pilot, and so oscillatory systems are acceptable. Instead, the fundamental limits of control can be employed to adjust the plant for best controller performance.

Strong disturbance rejection and fast response to input commands are desired for good performance. However, the 'water-bed effect' of the Bode

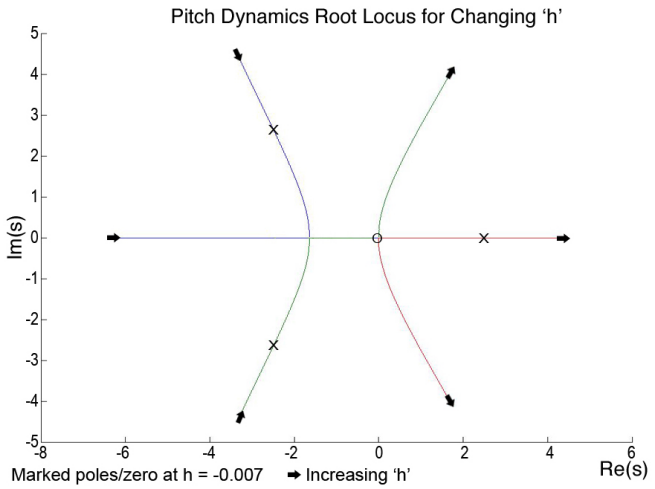

Figure 5: Root Locus of Pitch Dynamics for Changing Rotor Height Above CoG.

integral for the sensitivity function imposes a limit on arbitrary design targets for the controller across all frequencies: it states that any arbitrary reduction in the sensitivity of the system implies a corresponding increase in sensitivity over other frequencies [Seron *et al.*, 1997].

In the case of the X-4 Flyer, both low frequency disturbances, which cause drift, and high frequency disturbances, which induce noise in the inertial sensors, must be rejected. For this reason, it is desirable to reduce the integral of sensitivity function across the underlying system, prior to the application of any control.

The sensitivity function can be related directly to the poles of the open-loop plant through the Bode integral. From Seron *et al*:

$$\int_0^\infty \log|S(e^{j\omega})|d\omega = \pi \sum_{i=1}^{n_p} p_i \tag{47}$$

where S is the sensitivity function of the system, p_i are the poles of the open loop plant, and ω is frequency [Seron *et al.*, 1997].

Calculating the Bode integral for a range of h from -0.05 to 0.05 m below the rotor demonstrates a sharp notch at $h = 0$ (see Fig. 6). When the rotor plane is coincident with the center of gravity, the Bode integral is zero. In this configuration, the pitch dynamic is neutral.

The magnitude of the integral changes sharply as the rotor plane moves away from the CoG. Given the strong correlation between h error and plant

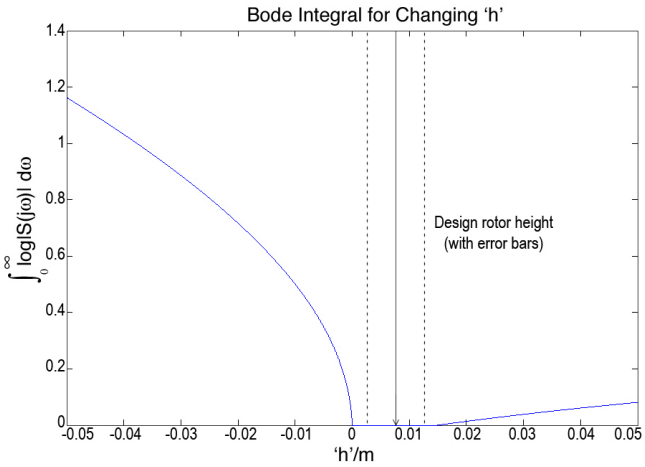

Figure 6: Bode Integral With Respect to Rotor Plane Placement.

structure, and the link between sensitivity and h position, it is clear that close attention to the correct tuning and verification of rotor height is essential for the performance of the helicopter.

For the X-4 Flyer, the ideal rotor position is at $h = 0$. However, as the root locus with changing h demonstrates, the structure of the plant undergoes significant change with error around this point. For this reason, the CoG is set slightly away from the rotor plane so that small errors will not have an impact on stability. The Bode integral corresponding to the rotor position, with error bars, is shown on Fig. 6. Although more difficult to control by a human, this choice maximises the achievable performance of the closed-loop system.

6. Attitude Control

Quadrotor attitude control has been well researched by groups at many universities. A variety of control techniques has been implemented successfully on quadrotor UAVs — PID, LQ, feedback linearisation, nonlinear PD and PD^2 [Bouabdallah *et al.*, 2004b], backstepping [Guenard *et al.*, 2005], adaptive nonlinear control, sliding-mode [Waslander *et al.*, 2005] and robust control.

In practice, the performance of simple control schemes are competitive with even very complex schemes. The dynamic regulation performance of most controllers is within $\pm$ 2 degrees of level tracking, and the best in the

range of ± 0.5 to 1 degrees. It is the authors' assertion that the limiting factor in quadrotor dynamic control is the performance of the actuators. It has been suggested that less complicated designs such as PID may, in fact, offer an advantage due to their simplicity and potential robustness to parameter variation [Bouabdallah *et al.*, 2004b]. These qualities are desirable for our full flapping model which is especially sensitive to changes in h.

In addition to the attitude dynamics, the X-4 Flyer also has important motor dynamics. The motor dynamics act in series with the rigid body dynamics – fast motor response is important for authoritive attitude control of quadrotors. To this end, rotor speed controllers have been developed to improve the natural performance of the rotor-motor system [Pounds *et al.*, 2009]. The linearised closed-loop motor system transfer function, $H_{\text{M-CL}}$, is:

$$H_{\text{M-CL}} = \frac{68.85(s + 0.42)}{(s + 78.46)(s + 0.44)} \tag{48}$$

6.1. Discretised Model

The controller runs at 50 Hz, the maximum frequency at which attitude data is updated, and so the dynamics of the plant are discretised at $t_{\text{s}} = 0.02$ seconds for the control design. The IMU returns both angle and rate information, which allows for a PID controller in the improper form $C = k(1 + i/s + ds)$ to be realised, where C is the controller transfer function, k is the proportional system gain, i and d are the integral and differential scalings and e is the system error. The complete discretised model, $G_{\text{c}} = \theta/\delta\omega$, is:

$$G_{\text{c}} = \frac{1.4343 \times 10^{-5}(z - 0.9916)(z + 1)(z - 0.9997)}{(z - 0.2082)(z - 0.9914)(z - 1.038)(z^2 - 1.943z + 0.9448)} \tag{49}$$

where $\delta\omega$ is the differential variation in rotor speed about the operating condition, 850 rad·s^{-1}. The additional zero at $z = -1$ comes from the matched pole-zero discretisation method.

6.2. Controller Design

The proposed controller consists of a discrete PID controller. The transfer function of the controller, C, is:

$$\text{C} = 400\left(1 + 0.2\frac{0.02}{(z - 1)} + 0.3\frac{(z - 1)}{0.02}\right) \tag{50}$$

As the motor dynamics are so fast, the dominant pole has little interaction with the attitude mechanics. If it were slower, the excess poles would diverge closer to the unit circle, leading to oscillation and possibly instability. The slow motor pole-zero cancellation is associated with the dynamics of the lithium ion polymer cells, and sufficient gain causes the pole to close with the zero.

7. Flight Testing and Performance

The X-4 underwent extensive testing prior to free flight outdoors. With the exception of the outdoor flight, all tests were performed in a test cage in the ANU Mechatronics Laboratory. The X-4's high speed rotors are quite dangerous and untethered indoor and outdoor flights were not attempted until confidence in the vehicle was established. Prior to the designed controller being tested under flight conditions, controller functionality was validated with the X-4 fixed on a gimbal rig at low rotor speed [Pounds *et al.*, 2006].

For testing with translational freedom the aircraft was suspended just above the ground at start-up and then the controller was turned on as the rotors were brought up to flight speed. Integral gain was previously turned off to avoid wind-up conditions during testing. In this test the attitude controller was:

$$\mathrm{C} = 400\left(1 + 0.3\frac{(z-1)}{0.02}\right) \tag{51}$$

The zero integral gain caused the flyer to stabilise at non-zero angles. The X-4 lifted itself in ground effect (0.4 m) and regulated its attitude within ± 1 degree of equilibrium (see Fig. 7).

For testing beyond ground effect the X-4 was flown tethered indoors. After engaging the attitude controller the suspended flyer was hoisted up 1.5 m into the air before bringing the rotors to flight speed. A pilot sent attitude reference commands to the flyer to keep it centered in the test area; the pilot did not stabilise the vehicle. The X-4 flew at a height of approximately 2 m (see Fig. 8).

The outdoor test took place on an ANU sports field. A smooth platform was used for take-off to allow the flyer to slide sideways freely rather than catch and flip. To avoid integrator wind-up, the X-4 was brought up to flight speed, then hopped into the air under manual mode before switching to autonomous control. During the flight a pilot sent commands to the flyer to control throttle but did not stabilise the vehicle. The X-4 took off

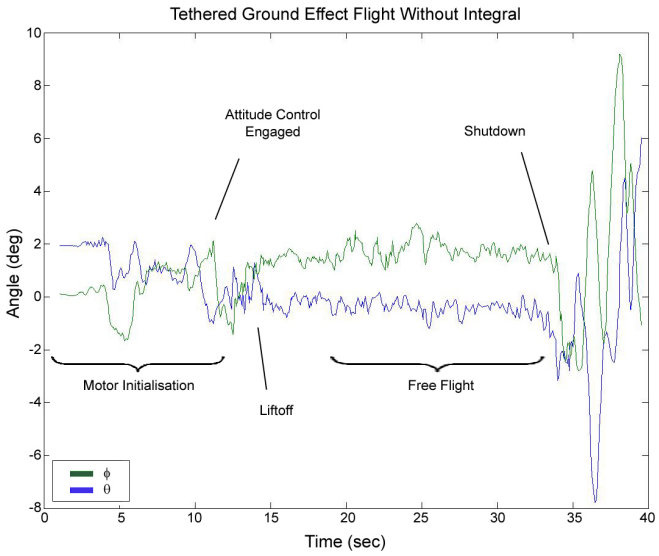

Figure 7: Pitch and Roll Stabilisation in Ground Effect.

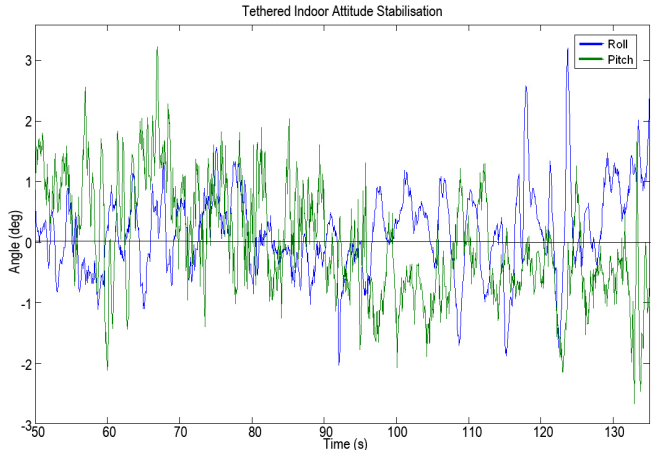

Figure 8: Tethered Indoor Pitch and Roll Stabilisation.

Figure 9: The X-4 Flyer in Outdoor Flight.

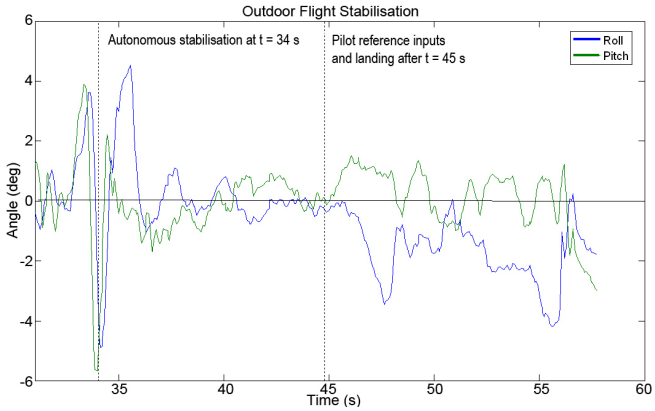

Figure 10: Outdoor Flight Autonomous Pitch and Roll Angle Stabilisation.

from the ground and flew to above 2 m and stayed airborne for 25 seconds (see Fig. 9). For ten seconds of the flight, the pilot made no stick corrections. In this time the flyer regulated its attitude within ± 1 degrees of level for 5 seconds (see Fig. 10).

8. Conclusion

A 4 kg quadrotor with a 1 kg payload was demonstrated in flight. From the analysis of flyer attitude dynamics with flapping, the mechanical design was tuned for best control sensitivity and disturbance rejection. A PID controller was designed to stabilise the dominant decoupled pitch and roll modes. In practice the craft was capable of stabilising itself in indoor flight

with $\pm$ 1 degree of level precision, and outdoors in a short flight with comparable attitude precision. However, extensive tests have yet to be conducted. To the authors' knowledge, this is the first successful outdoor test of a >4 kg quadrotor UAV.

The X-4 project is now concluded, but many lessons about practical large quadrotor development have been learned. It was seen that good control and careful plant design are important for realising good system performance, especially for slow, bandwidth limited craft. The next steps in developing this system include further exploration of rotor dynamics unique to quadrotors, and modernising motors, batteries and avionics. Newer IMU systems have the potential for pushing system control performance with sample times above 100 Hz.

9. Acknowledgements

The authors would like to thank CSIRO ICT Robotics and Ryan Pope for their ongoing support of this project.

References

J Borenstein. The hoverbot — an electrically powered flying robot. 1992. ftp://ftp.eecs.umich.edu/people/johannb/paper99.pdf.

S Bouabdallah, P Murrieri, and R Siegwart. Design and control of an indoor micro quad-rotor. *Proc. International Conference on Robotics and Automation*, 2004.

S Bouabdallah, A Noth, and R Siegwart. Pid vs lq control techniques applied to an indoor micro quadrotor. *Proc. IEEE/RSJ International Conference on Intelligent Robots and Systems*, 2004.

N Guenard, T Hamel, and V Moreau. Dynamic modeling and intuitive control strategy for an "x4-flyer". *Proc. 5th International Conference on Control and Automation*, 2005.

T Hamel, R Mahony, R Lozano, and J Ostrowski. Dynamic modelling and configuration stabilization for an x4-flyer. *Proc. 15th Triennial World Congress of the International Federation of Automatic Control*, 2002.

H Huang, G Hoffman, S Waslander and C Tomlin. Aerodynamics and Control of Autonomous Quadrotor Helicopters in Aggressive Maneuvering. In *Proc. 9th International Conference on Robotics and Automation*, 2009.

JG Leishman. *Principles of Helicopter Aerodynamics*. Cambridge University Press, Cambridge, United Kingdom, second edition, 2006.

Ascending Technologies GmbH, 2009. http://www.asctec.de/main/index.php.

Draganfly Innovations Inc, 2009. http://www.draganfly.com/.

E Nice. *Design of a Four Rotor Hovering Vehicle*. PhD thesis, Cornell University, 2004.

P Pounds, R Mahony, and P Corke. Modelling and Control of a Quadrotor Robot. *Proc. Australasian Conference on Robotics and Automation*, 2006.

P Pounds, R Mahony, and P Corke. Design of a static thruster for micro air vehicle rotorcraft. *Journal of Aerospace Engineering*, 22, 2009.

RW Prouty. *Helicopter Performance, Stability and Control*. Krieger Publishing Company, London, United Kingdom, first edition, 2002.

M Seron, J Braslavsky, and G Goodwin. *Fundemental Limitations in Filtering and Control*. Springer-Verlag, London, United Kingdom, first edition, 1997.

S Waslander, G Hoffmann, J Jang, and C Tomlin. Multi-agent quadrotor testbed control design: Integral sliding mode vs. reinforcement learning. *Proc. IEEE/RSJ International Conference on Intelligent Robots and Systems*, 2005.

10. Figure Captions

.

Figure 1: The X-4 Flyer.
Figure 2: Flapping Quadrotor Free-body Diagram.
Figure 3: Blade Flapping Angle Rotation.
Figure 4: X-4 Component Offsets.
Figure 5: Root Locus of Pitch Dynamics for Changing Rotor Height Above

	Value	Error	Unit
a_0	5.5	± 0.5	
c_{tip}	0.012	± 0.001	m
m	4.34	$\pm 5 \times 10^{-3}$	kg
A	0.0855	$\pm 0.1 \times 10^{-3}$	m^2
C_T	0.0047	$\pm 0.2 \times 10^{-3}$	
C_Q	0.228×10^{-3}	$\pm 0.015 \times 10^{-3}$	
I_b	40.887×10^{-6}	$\pm 3.655 \times 10^{-6}$	$\mathrm{kg \cdot m}^2$
r	0.165	$\pm 0.5 \times 10^{-3}$	m
ρ	1.184	Not available	$\mathrm{kg \cdot m}^{-3}$
γ	1.417	± 0.133	
λ	0.049	$\pm 2 \times 10^{-3}$	
θ_{tip}	4.4	± 0.5	deg
σ	0.054	$\pm 1 \times 10^{-3}$	
ω_hover	850	± 5	$\mathrm{rad \cdot s}^{-1}$

Table 1: Aerodynamic Parameters and Associated Error.

CoG.
Figure 6: Bode Integral With Respect to Rotor Plane Placement.
Figure 7: Pitch and Roll Stabilisation in Ground Effect.
Figure 8: Tethered Indoor Pitch and Roll Stabilisation.
Figure 9: The X-4 Flyer in Outdoor Flight.
Figure 10: Outdoor Flight Autonomous Pitch and Roll Angle Stabilisation.

11. Tables

	Part	mass/kg	d/m	e/m	h/m
A	Avionics	0.242	0	0	-0.02
B	Rotor	0.046	0.315	0	0
C	Motor	0.288	0.315	0	-0.06
D	ESC	0.074	0.15	0.035	-0.055
E	Powerbus	0.099	0	0	-0.13
F	$\text{Batt}_{\text{long}}$	0.165	0.0125	0.06	0.035
G	Batt_{lat}	0.165	0.0	0.04	0.035
H	Arm	0.039	0.157	0.035	0.04
I	Hoop	0.200	0	0	-0.17

Table 2: Component Masses and Offsets.

	Value	Error	Unit
I_{XX}	0.0820	± 0.0025	$\text{kg}\cdot\text{m}^2$
I_{YY}	0.0845	± 0.0029	$\text{kg}\cdot\text{m}^2$
I_{ZZ}	0.1377	± 0.0059	$\text{kg}\cdot\text{m}^2$

Table 3: Diagonal Inertial Elements.

	Value	Error
p_1	$-2.507 + 2.671i$	$\pm 0.714 + 1.244i$
p_2	$-2.507 - 2.671i$	$\pm 0.714 + 1.244i$
p_3	2.578	± 1.129
z	-0.015	± 0.003

Table 4: Poles and Zeros of the Open Loop Pitch Dynamics.